Energy 91 (2015) 451–464

Contents lists available at ScienceDirect

Energy

journal homepage: www.elsevier.com/locate/energy

Application of the steady flamelet model on a lab-scale and an industrial furnace for different oxygen concentrations

Rene Prieler [a, *], Bernhard Mayr [a], Martin Demuth [b], Davor Spoljaric [b], Christoph Hochenauer [a]

[a] Institute of Thermal Engineering, Graz University of Technology, Inffeldgasse 25/B, A-8010 Graz, Austria
[b] Messer Austria GmbH – Kompetenzzentrum Metallurgie, Industriestraße 5, A-2352 Gumpoldskirchen, Austria

ARTICLE INFO

Article history:
Received 12 December 2014
Received in revised form
23 June 2015
Accepted 17 August 2015
Available online xxx

Keywords:
Oxygen enriched combustion
Reheating furnace
Computational fluid dynamics
Energetic efficiency
Steady flamelet

ABSTRACT

In the present study a numerical and experimental investigation was done on the impact of oxy-fuel combustion in a lab-scale furnace. For combustion and radiation modelling the steady flamelet approach with 17 species and 25 reactions associated with a WSGG (weighted sum of grey-gases) model was used. CFD (computational fluid dynamics) model was validated by measured temperatures and heat fluxes with different O_2 concentrations. It was found that simulated temperatures and heat fluxes were in close agreement with the measurements in the full range of oxygen enrichment. Although 17 species were considered the calculation time was significantly reduced by the steady flamelet approach compared to commonly used eddy dissipation concept models. Predicted and measured data revealed gas savings of 8.2% by an O_2 concentration of 25 vol% instead of 21 vol%. Maximum gas savings were determined for 100 vol% O_2 with a value of 16.7%. The CFD model was also applied to a simulation of an 18.2 MW walking hearth furnace under air-fired conditions which should be adapted for oxy-fuel combustion in the future. Results from CFD showed a heat flux of 9.15 MW compared to the required 9.33 MW according to the material data and production rate.

1. Introduction

The combustion of fossil fuels, currently the most important source of the anthropogenic greenhouse gas CO_2, is a key process in a number of different applications like power generation, transportation and several industrial sectors. Nowadays, proven by several studies, the reduction of CO_2 emissions is identified as main topic to reduce the global warming. The IPCC (Intergovernmental Panel on Climate Change) determined the total amount of CO_2 emissions from fossil fuels in the year 2000 to be 23.5 Gt/a, where about 60% were produced by large scale plants with emissions of more than 0.1 Mt/a [1]. CO_2 can also arise as a side product in several industries like cement and glass melting. Manickam et al. [2] quantified that about 68% of the CO_2 in cement clinker formation is formed by carbonates and that the rest emerges by combustion. The same trend was observed by Falcitelli et al. [3] in two glass melting furnaces where 30 to 36 vol% of the overall CO_2 emissions was emitted from the glass bath. Therefore, decreasing CO_2 emissions is inevitable for the main emitting industries to slow down the global warming. Oxy-fuel or oxygen enriched combustion represents a technological option for CCS (carbon capturing and storage) to avoid CO_2 emissions besides pre- and post-combustion. Actually, most investigations regarding oxy-fuel combustion have been related for application in power plants which use pulverized coal as fuel. Detailed reviews for oxy-coal combustion were already published by Chen et al. [4], Scheffknecht et al. [5] and Wall et al. [6].

Besides environmental issues, for high temperature processes like melting and annealing furnaces, with a huge demand on fossil fuels, the increase of the energetic efficiency is also crucial. Due to the absence of nitrogen in the oxidizer for oxy-fuel combustion a lower fuel input is needed to reach the same flame temperature as for the conventional air-fired case. Furthermore, high H_2O and CO_2 concentrations lead to improvements on the heat transfer in boilers and furnaces through enhanced radiation intensity which causes a more homogeneous temperature distribution and product quality (i.e. cement, glass, steel …). Moreover, the flow-rate of the flue gas and CO_2 emission can be decreased. On that account, oxy-fuel

* Corresponding author. Tel.: +43 316 873 7810.
E-mail address: rene.prieler@tugraz.at (R. Prieler).

http://dx.doi.org/10.1016/j.energy.2015.08.070
0360-5442/

technology can be an upcoming technology to reduce greenhouse gas emissions and simultaneously reach higher efficiency levels. Oliveira et al. [7] carried out an analysis with simple energy balances about fuel saving in metal reheating furnaces using oxy-fuel combustion. It was calculated that at a temperature level of 1200 °C the fuel consumption could be reduced by 46% if pure oxygen is used instead of air (without pre-heating of the oxidizer). Oxygen enhanced combustion was also investigated by experiments on a test facility by Bělohradský et al. [8]. Increasing the oxygen content in the oxidizer up to 46 vol% leads to an improvement of the combustion efficiency of 22%. Beside the advantages of oxy-fuel combustion some technical efforts, like O_2 production or an additional process unit to obtain the desired O_2 concentration in the oxidizer, has to be conquered on the implementation in existing firing systems in industry. Commercial production technologies for O_2 are cryogenic air separation, vacuum swing adsorption etc. and are summarized in Baukal [9]. Nevertheless, many industrial processes use oxygen and therefore on-site oxygen production is available for example in steel industry. Further consideration has to be done on the furnace to prevent air leaking and overheating of the burners and refractory due to higher flame temperature in oxy-fuel combustion. An overview about the advantages and implementation of oxy-fuel combustion is given in Ref. [9].

Recent developments in computer power allow numerical investigations of a huge number of manufacturing processes with reasonable effort. Several studies about the modelling of combustion processes were carried out with different approaches like reactor network systems or CFD (computational fluid dynamics). Reactor network systems offer a simple method to analyse gas phase combustion in furnaces. Ponsich et al. [10] carried out a reactor network analysis of a glass melting furnace to predict the residence time distribution of the gas phase and the glass bath. A comparison with a CFD simulation showed similar results with the benefit of a lower computational demand. Important spatial information about the flow field, temperature distribution and species concentration are not calculated by such reactor network analysis. Falcitelli et al. [3] conducted a hybrid CFD/reactor network analysis of two different glass melting furnaces (5 and 10 MW fuel input) to predict the NOx emissions. First, a CFD simulation was done with a reduced reaction mechanism, involving the main species. Based on the CFD results a reactor network analysis was performed with detailed chemical kinetics for the combustion of natural-gas including a sub-model for nitrogen (about 3200 reactions and 240 species overall). NOx values at the furnace outlet showed a close agreement of measured and calculated data. In high temperature applications knowledge about the heat transfer is essential for the dimensioning and operating of the furnace. The CFD model is able to predict the heat transfer as well as detailed resolution of the flow field inside the combustion chamber especially when measurements of temperature and species concentrations are difficult. Habibi et al. [11] for example, investigated the heat flux and NOx concentrations in a steam cracking under air-fired conditions. Another study on flow, combustion and heat transfer was done by Guihua et al. [12] for an ethylene cracking furnace. The effect of the heat transfer on the cracking process was shown by coupling of the CFD model with the thermal cracking process. With regard on oxy-fuel combustion, several numerical studies were carried out on lab-scale and industrial furnaces for different applications. A rotary kiln for cement manufacturing was simulated by Manickam et al. [2] with oxygen enriched combustion of coal with special emphasis on the flame shape. Furu et al. [13] tested the impact of different oxygen enrichments on the heat transfer to aluminium samples in a pilot scale furnace by measurement and CFD. Improved heat transfer to the samples was determined using the oxy-fuel conditions in the furnace.

Nowadays, most commercial CFD codes offer a big selection of models to consider transport phenomena in furnaces. Depending on the application and combustion environment, the choice of appropriate models to describe the combustion is important for accurate predictions of transport problems. It was found that chemistry and radiation modelling are the crucial parts in CFD simulations of combustion processes. The majority of the models for radiation and chemistry calculation in CFD were developed and optimized for air-fired conditions. High flame temperature, H_2O and CO_2 concentrations in oxy-fuel combustion lead to different combustion phenomena due to dissociation effects and the radiative properties of the flue gas. The aim is to find suitable combustion and radiation models which are applicable in the full range of oxygen enrichment as well as air-firing systems.

Computational costs for detailed CFD analysis of the chemical kinetic in a combustion chamber are still high, especially when the furnace exceeds lab-scale sizes. On that account most researchers use reduced chemical reaction mechanisms to predict the combustion. Although detailed mechanisms like the GRI3.0 [14] involve more than 300 reactions and 50 species, global mechanisms with just a few reaction steps seem to be sufficient for air-natural-gas combustion. For example WD (Westbrook and Dryer) [15] and JL (Jones and Lindstedt) [16] proposed 2-step and 4-step mechanisms which were successfully used in the past for combustion with air. In such global mechanisms only the main species are included. Due to high flame temperature in oxy-fuel combustion the formation of radicals like H, O and OH has to be considered. This statement was demonstrated by simulations for an oxy-fuel and air-fuel counter-flow diffusion flame by Frassoldatti et al. [17]. A comparison with a detailed chemical kinetic showed that WD and JL mechanisms failed to predict the adiabatic flame temperature of the oxy-fuel case in a range of 0.4–2 for the equivalence ratio. The flame temperature was overestimated by the global mechanisms due to the neglected radicals. However, results with global and detailed mechanisms were similar for air-fired conditions. An adaptation of the JL mechanism, which involves radicals, leads to improved prediction of the adiabatic flame temperature. Yin et al. [18] calculated same the results for the adiabatic flame temperature in oxy-fuel and air-fuel combustion between equivalence ratios of 0.6 and 1.4. A CFD simulation with a refined JL mechanism calculated close results to measurements of temperature and species on a 0.8 MW IFRF furnace. Glarborg and Bentzen [19] also considered hydrocarbon radicals in their investigations. It was found that CO occurs at high temperatures due to dissociation of CO_2 because of the presence of radicals and thermal dissociation. Andersen et al. [20] performed calculations on an isothermal plug-flow reactor as well as a CFD simulation of a propane-oxygen flame with refined mechanisms. Results for both calculations determine the influence of radicals in oxygen enriched combustion. The impact of chemical kinetics on the calculation time was investigated by Tihay et al. [21]. Global and skeletal reaction mechanisms, up to 20 species and 49 reactions, were tested in the study. A skeletal mechanism proposed by Peters and Kee [22] showed the best results with reasonable computational demand, however it was stated that detailed skeletal mechanisms are still too time intensive for use in combustion modelling. Since the impact of radicals on oxy-fuel combustion was determined, Prieler et al. [23] tested three detailed reaction mechanisms with 17 and 53 species respectively. The steady flamelet approach was used, where chemistry calculations were done before the CFD simulations to keep the computational effort to a minimum. Results revealed that the skeletal25 mechanism [24] was able to predict the flame shape and achieved good accordance with temperature measurement. Based on the mentioned publications, it can be concluded that the presence of

radicals in high temperature processes has a vast influence on accurate prediction of temperature and species concentrations in CFD.

Knowledge about the heat transfer in furnaces mainly promoted by radiation is the second crucial part in the understanding of combustion processes. Depending on the flue gas composition and temperature the radiation intensity is significantly different. Commonly used CFD codes simulate the radiative properties of gases with the assumption of one grey gas without the spectral dependence of their components. In air-fuel cases, where the nitrogen concentration is high compared to CO_2 and H_2O, this approach seems to be accurate enough. However, this consideration tends to fail when nitrogen concentration in the flue gas decreases in oxygen enriched combustion. High levels of CO_2 and H_2O in an oxy-fuel environment (with or without recycled flue gas) lead to special consideration of the radiative properties by a non-grey gas approach. A differentiation also has to be made between oxy-fuel combustion in annealing and melting furnaces as well as boilers in power plants. In power plants recycled flue gas is used to control the flame temperature during the combustion because of material limits (e.g. about 1600 K for gas turbines [25]). In cement, steel and glass industries high temperatures are desired. Therefore the partial pressure ratio of H_2O and CO_2, and by association the radiative properties of the flue gas, are addicted to the operating conditions and application of the furnace. There are three main approaches to describe the radiative properties: the LBL (line-by-line) method, band models and global methods. A line-by-line model is the most accurate approach but computationally demanding and not applicable in CFD for combustion modelling of large scale furnaces. Instead, global methods like the WSGGM (weighted sum of grey-gases model) proposed by Hottel and Sarofim [26] are commonly used for combustion modelling under air-fuel conditions because of their low computational demand. Porter et al. [27] carried out calculations with the WSGG (weighted sum of grey-gases) model and the FSCK (full spectrum correlated k-distributions) method [28–30] for grey and non-grey treatment of the gas under air-fuel and oxy-fuel conditions. Results were compared to the SNB (statistical narrow band model) [31]. Based on the data, the use of a non-grey approach for oxy-fuel conditions is recommended to combustion modelling. Becher et al. [32,33] validated LBL models (from HITEMP2010 [34], HITEMP1995 [35], HITRAN2008 [36] and HITRAN2004 [37]) and band models (from RADCAL [38], EM2C [39] and EWB [40]) by gas cell experiments. Highest accuracy was found with results from HITEMP2010. These data were also compared to the global WSGG model with different coefficients. A maximum deviation of 59% in oxy-fuel environment was observed for WSGGM parameters by Smith et al. [41], which are widely used. On that account, many researchers have published new WSGGM's for oxy-fuel combustion recently. For example Yin et al. [42] proposed new coefficients for the WSGG model which are valid for different partial pressure ratios of CO_2 and H_2O. These parameters were tested for oxy-fuel and air-fuel combustion and compared to coefficients from Ref. [41]. Validation of the new WSGGM coefficients was done by comparison with an EWBM (exponential wide band model) [43] which were in close agreement for the air-fired and oxy-fuel cases. Further WSGG model parameters for oxy-fuel combustion were proposed by Johansson et al. [44,45], Bordbar et al. [46], Rehfeldt et al. [47], Kangwanpongpan et al. [48] and Krishnamoorthy [49].

The different approaches for chemistry and radiation modelling in oxygen enriched combustion were already used for CFD simulations of lab-scale and industrial furnaces. Yin et al. [18] investigated a 0.8 MW furnace and a 609 MW boiler with two WSGG models (see Ref. [42]) and refined global reaction mechanisms of WD [20] and JL [50]. Simulation of the 0.8 MW furnace showed negligible impact of the WSGG models for this small beam length. In contrast to the small scale furnace, the WSGG models that were used had a high impact on the simulation results of the 609 MW boiler. The simulations were carried out with the EDC (eddy dissipation concept) model which is computationally demanding compared to the steady flamelet approach. Al-Abbas and Naser [51,52] conducted experiments and CFD simulations on a 100 kW propane-fired and coal-fired furnace. Air-fired and different oxy-fuel cases with recycled flue gas were investigated. One- and four-step reaction mechanisms with the eddy break-up model were applied for the simulation and compared to measured temperature and species concentrations. Closer agreement with measured data was observed with the four-step mechanism due to a more accurate prediction of the CO/CO_2 production rate and H_2/H_2O equilibrium especially in the main reaction zone. The studies showed that dissociation effects in oxy-fuel combustion will have to be considered inevitably. It has to be mentioned that the model parameters has to be adapted for each case (air-fuel and oxy-fuel). Galletti et al. [53] simulated a 3 MW semi-industrial furnace with refined global reaction mechanisms for oxy-fuel conditions by Andersen et al. [20] and two WSGG models with coefficients from Coppalle et al. [54] and Johansson et al. [44]. For combustion modelling the EDC and EDM (eddy dissipation model) were used. A comparison of different combustion models (EDC, EDM and steady flamelet model) with respect on the calculation time is given in Ref. [23].

Reduction of CO_2 emissions as well as increased plant efficiency, combined with natural-gas savings, will be crucial aspects for plant operations in the future for several industries. Oxy-fuel technology can help to achieve these economic and environmental goals. In times of increasing computer power, numerical tools like CFD are used to predict the effect of oxygen enrichment on the production rate and avoid expensive test runs at the same time. A numerical and experimental study of the increase in furnace efficiency due to oxygen enriched combustion was done by Prieler et al. [55]. They measured and simulated the heat transfer to the furnace load and highlighted the increase of furnace efficiency as well gas savings in a range of 25–100 vol% O_2 in the oxidizer. Literature research revealed many investigations on chemistry and radiation for oxy-fuel combustion in lab-scale and industrial dimensions. Most publications investigated global reaction mechanisms with just the main species. It was pointed out in this section that the considerations of intermediate species like radicals, CO/CO_2 equilibrium etc. is an important topic in combustion modelling in an oxy-fuel environment. Therefore, the main emphasis of this paper was to use a detailed chemical kinetic and WSGG model for combustion modelling in a lab-scale furnace in a range of 41.7–97 kW and an 18.2 MW walking hearth furnace to reheat steel billets. Simulations were done using the commercial software package ANSYS Fluent. The steady laminar flamelet model was applied to reduce the calculation time compared to used EDC and EDM by the other researchers. The numerical model that was used was tested on the lab-scale furnace with air-fuel and 4 oxy-fuel combustion cases. CFD prediction was validated by measured temperature and heat transfer to the furnace load. Based on the results, the furnace efficiency and gas savings were investigated for two different temperature levels. The 18.2 MW walking hearth furnace was operated just under an air-fuel environment. Heat transfer to the steel billets inside the furnace was simulated by CFD and compared with an analytical calculation of the heating process. A simulation of the walking hearth furnace for natural-gas/air combustion was done to validate the combustion model on industrial furnace dimensions. This simulation will be the basis for oxygen enriched simulations and optimization activities on the furnace.

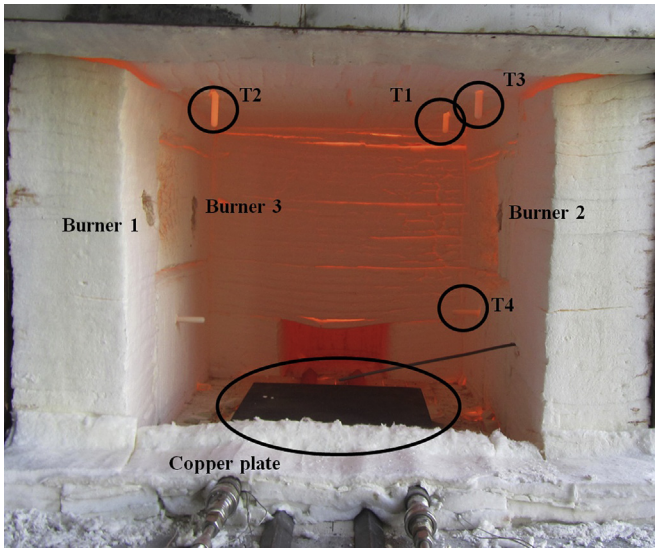

Fig. 1. Position of the thermal sink and thermocouples T1, T2, T3 and T4 in the lab-scale furnace.

2. Experimental setup

2.1. Lab-scale furnace

The lab-scale furnace was operated with three "Messer Oxipyr®-Flex" burners with a maximum fuel input of 33 kW natural-gas per burner. The main dimensions of the combustion chamber, which was surrounded by a ceramic insulation of 200 mm thickness, were 0.77 × 0.75 × 0.99 m. Experiments were carried out with oxygen concentrations of 21, 25, 30, 45 and 100 vol% in the O_2/N_2 mixture. Operating conditions between 21 and 45 vol% were investigated in detail because higher increase of the flame temperature and furnace efficiency is expected in this range (see Refs. [9,55]). Operating pressure in the furnace was approximately 0.3 mbar higher than ambient pressure to avoid air leaking in oxygen enriched combustion. Although a positive pressure in the furnace was achieved, air leaking was detected by oxygen measurement in the dry flue gas because of small gaps between the front door and the walls as well as the position where the burners were attached to the furnace. Fig. 1 shows the investigated furnace with the thermal load and temperature measurements. Four Type B thermocouples were arranged inside the furnace. Thermocouples T1, T2 and T3 were inserted into the furnace through the top wall (above burner 1 to 3) through the ceramic insulation (see Fig. 1). T4 was placed at the right furnace wall. The furnace load in melting and annealing furnaces was represented by a water cooled copper plate which was coated with soot formed by a fuel-rich natural-gas flame before the experiments to maximize the emissivity. Thermal heat flux to the plate was determined by temperature measurement of the cooling water before and behind the plate. Four Type K thermocouples also measured the temperature 10 mm below the top surface of the plate.

2.1.1. Experiments without thermal load

First, tests runs were carried out without the thermal load inside the furnace to investigate the potential of gas savings for five different oxygen levels in the oxidizer (21, 25, 30, 45 and 100 vol% O_2). Only burner 2 was active during these experiments. The mass-flow-rate of natural-gas was adapted for each case to achieve the same temperature of approximately 1090 °C, indicated by T4, in the furnace. Burner 2 was operated with an equivalence ratio of 1 (except 1.17 for 100 vol% O_2) to keep the residual oxygen concentration in the dry flue gas to a minimum.

2.1.2. Experiments with thermal load

Furnace efficiency and heat flux to the load were examined in the experiments. Burners 1 to 3 were activated during the test runs with the copper plate. Investigations of the heat flux to the load were done with two different temperature levels in the furnace. As for the experiments in Section 2.1.1, thermocouple T4 was used to indicate the temperature level. Fuel input was adjusted until the temperature levels of 1000 °C and 1220 °C were reached for T4. The fuel input and equivalence ratio applied in the experiments are displayed in Table 1. During the experiments an average measured value at the thermal load of 130 °C (at 1000 °C) and 190 °C (at 1220 °C) was detected by the four Type K thermocouples. At a temperature level of 1220 °C the cases with 21 and 25 vol% O_2 were not realized because of the burner limit of 33 kW. Already at maximum burner power and 30 vol% O_2 it was not possible to reach the temperature level of 1220 °C in the experiments (measured 1193 °C).

2.2. Industrial walking hearth furnace

The second furnace, which was simulated by CFD, is an 18.2 MW walking hearth furnace for reheating steel billets. For symmetry reasons only one half of the furnace is shown in Fig. 2. Its main dimensions are 17 × 13 m and a height of 1.6 m, respectively. NG (Natural-gas) was supplied by 48 burners at the top wall of the furnace under air-fired conditions. Oxidizer (air) was preheated to 310 °C before entering the burner. The combustion chamber is subdivided into three zones which are colour marked by the burners in Fig. 2: pre-heating (yellow), heating (red) and soaking zone (orange). The pre-heating and heating zone are separated by a water cooled wall which passes through the entire width of the furnace. 64 steel billets with the dimensions of 0.12 × 0.12 × 12 m are loaded in the chamber. The billets were heated up from 20 to 1200 °C. Operating conditions of the furnace and material properties of the billets are given in Table 2.

3. Numerical model

3.1. Flow modelling

Reynolds-averaged Navier–Stokes equations for continuity and momentum (Eqs. (1) and (2)) were solved by using a double precision pressure-based (segregated) solver for the fluid flow. Further equations had to be solved for turbulence modelling. For the lab-

Table 1
Natural-gas consumption for all three burners and equivalence ratio for T4 temperatures of 1220 and 1000 °C.

	100 vol% O_2	45 vol% O_2	30 vol% O_2	25 vol% O_2	21 vol% O_2
Temperature 1220°C					
Natural-gas (kg/h)	5.33	6.26	6.98	–	–
Equivalence ratio	1.042	1.020	0.980	–	–
Temperature 1000°C					
Natural-gas (kg/h)	3.06	3.00	3.10	3.37	3.67
Equivalence ratio	1.020	1	1	1	1

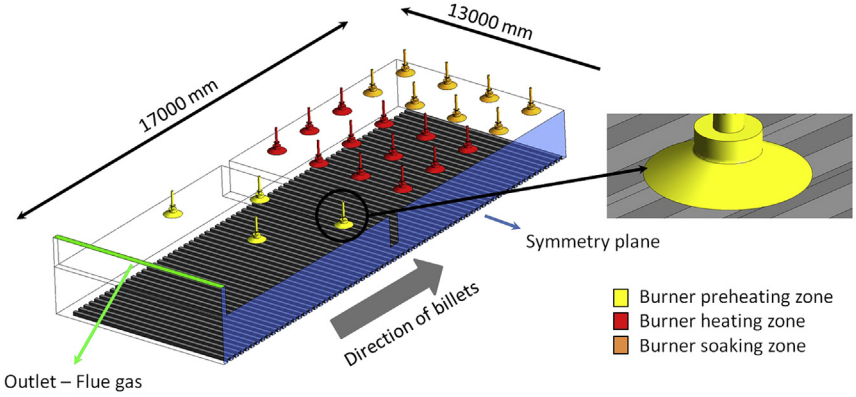

Fig. 2. 18.2 MW walking hearth furnace and detail view of the top wall burner in the pre-heating zone.

scale furnace the realizable k-epsilon model, proposed by Shih et al. [56], was used to calculate the dissipation rate and kinetic energy in two additional equations. The model settings applied in this study are given in Ref. [23]. It was found that the realizable k-epsilon model predicts temperature and species concentrations in close accordance to the RSM (Reynolds stress model) [57] and is therefore sufficient for the lab-scale application (see Ref. [55]). Spatial discretization of the scalars was done by the second order upwind scheme and PRESTO! was used to calculate the pressure. The SIMPLE algorithm was applied for pressure–velocity coupling. In the simulation, the flue gas was assumed to be an incompressible ideal gas, where density variation due to temperature was calculated by the ideal gas law. The operating pressure was set to 1013.25 mbar. The number of iterations was between 15 000 and 20 000 for each simulation approved by low residuals and constant monitors. All residuals were below a value of 10^{-3} especially for the mean mixture fraction, mixture fraction variance energy and radiation where values of approximately 10^{-6} were detected. Monitors were observed for the temperature and species concentrations at the outlet as well as the temperature at the measurement positions.

$$\frac{\partial}{\partial x_i}(\rho u_i) = 0 \tag{1}$$

$$\frac{\partial}{\partial x_j}(\rho u_i u_j) = -\frac{\partial p}{\partial x_i} + \frac{\partial}{\partial x_j}\left[\mu\left(\frac{\partial u_i}{\partial x_j} + \frac{\partial u_j}{\partial x_i} - \frac{2}{3}\delta_{ij}\frac{\partial u_l}{\partial x_l}\right)\right] + \frac{\partial}{\partial x_j}\left(-\rho\overline{u_i' u_j'}\right) \tag{2}$$

The only difference in flow modelling between the lab-scale and walking hearth furnace concerns the used discretization scheme and turbulence model. In contrast to the lab-scale furnace, high streamline curvatures occur in burner of the walking hearth furnace. Thus, the QUICK scheme for the spatial discretization (except second order for radiation) of the scalars and the RSM for the turbulence were used in the walking hearth furnace. The application of the RSM leads to higher computational demand due to 6 additional transport equations which have to be solved compared to the realizable k-epsilon model (two equations).

Table 2
Material properties of the billets and operating conditions.

Billets	
Density @ 20 °C (kg/m^3)	7800
Average specific heat (J/kg*K)	600
Production rate (t/h)	≈47.400
Operating conditions	
Temperature air (°C)	310
Temperature NG (°C)	25
NG pre-heating zone (kg/h)	≈290
NG heating zone (kg/h)	≈780
NG soaking zone (kg/h)	≈250
Equivalence ratio	0.97
O_2 concentration in the flue gas (vol%)	0.7

3.2. Boundary conditions and numerical grid

3.2.1. Lab-scale furnace

Pure methane and an O_2/N_2 mixture determined by the experiments were used to simulate the oxygen enriched combustion. All inlets were modelled by mass-flow-inlet conditions. Fuel mass-flow-rates and equivalence ratios for each simulation are given in Table 1. A porous zone was defined at the outlet to avoid backflows in the simulation. Temperature at the inlets was 25 °C. Hydraulic diameters were set to 3.5 and 4.5 mm at the fuel and oxidizer inlets. Different values for the turbulence intensity (5 and 20%) at the inlet were tested by Yin [58] for an oxy-fuel flame without differences for the predicted velocity, gas temperature and species concentrations and therefore a value of 10% was chosen for all simulations. A positive pressure of 0.3 mbar was calculated in the simulation by adapting the resistance of the porous zone at the outlet (see Fig. 3b). The material properties of the flue gas and solid materials in the model are summarized in Ref. [23]. The heat transfer to ambient was modelled by a convective boundary condition at the outer wall with a heat transfer coefficient of 30 W/m^2 K and a free stream temperature of 298.15 K.

The numerical grids for the CFD simulations with and without load are displayed in Fig. 3. The grid without load contains 630 413 cells (Fig. 3a). Fig. 3b shows the grid for the simulations with thermal load inside the furnace which consists of 1 431 339 elements. Grid independency tests for both meshes were done and the discretization error was estimated by a Richardson extrapolation [59]. The results of the Richardson extrapolation and additional information about the numerical grids can be found in Refs. [23,55].

The surfaces of the copper plate were defined with a temperature boundary condition in the CFD model. Temperatures and emissivities at the thermal sink which were used in CFD are given in Table 3.

3.2.2. Walking hearth furnace

Combustion of natural-gas in the furnace was modelled with methane and air (21 vol% O_2). The furnace geometry for the CFD simulation is displayed in Fig. 2 and operating conditions are given in Table 2. In contrast to modelling the lab-scale furnace, no porous

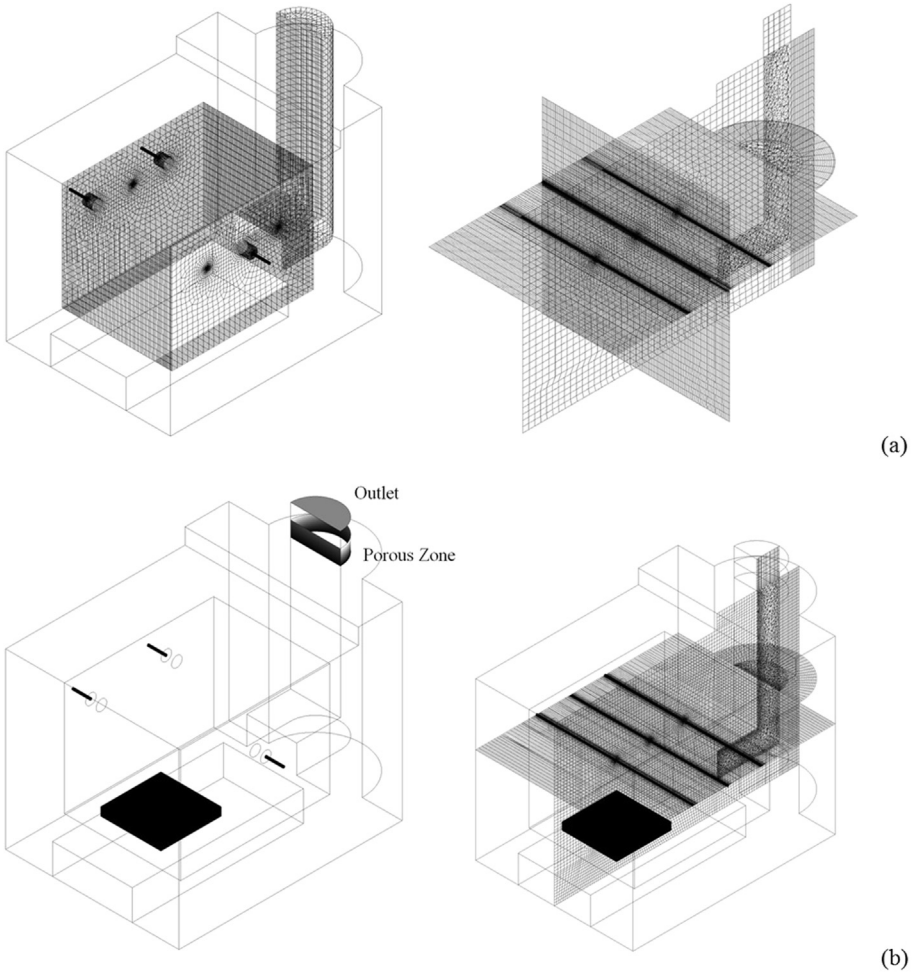

Fig. 3. CFD models of the lab-scale furnace: (a) without thermal load [23], (b) with thermal load [55].

zone was defined at the outlet. The hydraulic diameters were 0.11 and 0.0155 m for the methane and air inlets. Turbulence intensity was set to 10% at all mass-flow inlets. Solid furnace walls were not included in the CFD model to keep the number of cells to a minimum. Temperature boundary conditions at the furnace walls were defined by piecewise polynomial functions according to measurements with a quotient pyrometer. The measured values are summarized in Table 4. Emissivities were set to 0.9 and 0.3 for billet surfaces and walls. The computational grid for the walking hearth furnace consists of 4 972 260 cells. A further simulation with 8 026 188 cells showed marginal differences for temperature and species concentrations as well as heat fluxes in the furnace.

3.3. Combustion model

Chemistry modelling is a crucial part of an accurate numerical prediction of combustion processes. As mentioned in Section 1, the selection of a chemical reaction kinetic and their turbulence interaction can affect the calculated results especially under oxy-fuel conditions. Although adapted global reaction mechanisms with 4–6 reactions can predict oxy-fuel flames, a detailed chemical kinetic with consideration of radicals was applied for the combustion modelling. Widely used turbulence/chemistry interaction models are the EDM (eddy dissipation model) and EDC (eddy dissipation concept) model based on [60] and [61]. A numerical study on the applicability for oxy-fuel combustion was published by Prieler et al. [23]. It was found that, EDM was not able to calculate the oxy-fuel flame in accordance to the detailed EDC simulation. The disadvantage of the EDC model is the high calculation time for integrating the chemistry for each step.

In this study the SFM (steady laminar flamelet model), as a non-premixed approach, was used for turbulence/chemistry interaction. The chemistry integration was performed before the CFD simulation and the thermochemical state is subsequently related to the

Table 3
Boundary settings at the thermal load.

@1000 °C	
Temperature at boundary (°C)	130
Emissivity at boundary	0.5
@1220 °C	
Temperature at boundary (°C)	190
Emissivity at boundary	0.62

Table 4
Measured wall temperatures in the walking hearth furnace.

Measurement position (m)	Temperature (°C)
0	650
1.44	710
5.89	845
8.45	918
11.61	1179
16.06	1204
17.30	1200

enthalpy H and the mixture fraction f which is defined in Eq. (3), where Z_i, $Z_{i,ox}$ and $Z_{i,fuel}$ are the elemental mass fractions of element i in oxidizer and fuel [62,63].

$$f = \frac{Z_i - Z_{i,ox}}{Z_{i,fuel} - Z_{i,ox}} \tag{3}$$

SFM assumes that a turbulent flame can be simulated by an ensemble of small laminar diffusion flamelets. The state (temperature T, species concentrations Y_i) at each position in the flamelet is related to the mixture fraction. Such counter-flow diffusion flamelets were pre-processed with a detailed reaction mechanism. High computational demand due to chemistry integration during CFD was avoided. One-dimensional analysis was done with the flamelet equations given in Eqs. (4)–(6), where χ is the scalar dissipation, S_i is the reaction rate of species i, H_i is the specific enthalpy of species i, a_s is the strain rate and ρ_∞ stands for the density at the oxidizer inlet. In the present work the skeletal25 [24] reaction mechanism with 17 species and 25 reversible reactions was used for the flamelet calculations because of the applicability for different oxygen enrichments (see Ref. [55]). The reactions and species of the mechanism are summarized in Table 6 in the appendix.

$$\rho\frac{\partial Y_i}{\partial t} = \frac{1}{2}\rho\chi\frac{\partial^2 Y_i}{\partial f^2} + S_i \tag{4}$$

$$\rho\frac{\partial T}{\partial t} = \frac{1}{2}\rho\chi\frac{\partial^2 T}{\partial f^2} - \frac{1}{c_p}\sum_i H_i S_i + \frac{1}{2c_p}\rho\chi\left[\frac{\partial c_p}{\partial f} + \sum_i c_{p,i}\frac{\partial Y_i}{\partial f}\right]\frac{\partial T}{\partial f} \tag{5}$$

$$\chi = \frac{a_s}{4\pi}\frac{\left(\sqrt{\frac{\rho_\infty}{\rho}}+1\right)^2}{2\sqrt{\frac{\rho_\infty}{\rho}}+1} exp\left\{-2\left[erfc^{-1}(2f)\right]^2\right\} \tag{6}$$

Governing transport equations are solved for the Favre-averaged values of the scalars in the turbulent fluid flow. Thus, the relationship of instantaneous and average values of the scalars (temperature, species concentrations and density) has to be considered by a turbulence/chemistry interaction model. A presumed β-PDF (probability density function) $p(f)$ was used which represents the fraction of time that the fluid is in the state f. Average values of the scalars $\overline{\phi}_i$ were calculated by Eq. (7), where $\overline{H}$ is the Favre-average enthalpy and ϕ_i is the instantaneous value of the scalar. Furthermore, the mixture fraction variance $f^{''}$ [64] was used for the integration of the PDF $p(f)$. Mixture fraction variance is defined by Eq. (8), where f and $\overline{f}$ are the instantaneous and mean mixture fraction. The flamelet equations were solved and the PDF's were integrated before the CFD simulation and results of the Favre-average scalars (temperature, species concentrations and density) were stored in look-up tables.

$$\overline{\phi_i} = \int_0^1 p(f)\phi_i(f,\overline{H})df \tag{7}$$

$$f' = f - \overline{f} \tag{8}$$

All chemistry calculations were pre-processed without solving the complex flow field in the furnace. Although a detailed reaction mechanism with 17 species was applied, just two additional transport equations for f and $f^{''}$ have to be solved (see Eqs. (9) and (10)), where μ_t is the turbulent viscosity and σ_t, C_g and C_d are model constants given in Ref. [23]. Transport equation for the mean enthalpy is given in Eq. (11), where k_t is the turbulent conductivity and S_h is the source term.

$$\frac{\partial}{\partial t}\left(\rho\overline{f}\right) + \nabla\bullet\left(\rho\overrightarrow{v}\overline{f}\right) = \nabla\bullet\left(\frac{\mu_t}{\sigma_t}\nabla\overline{f}\right) \tag{9}$$

$$\frac{\partial}{\partial t}\left(\rho\overline{f'^2}\right) + \nabla\bullet\left(\rho\overrightarrow{v}\overline{f'^2}\right) = \nabla\bullet\left(\frac{\mu_t}{\sigma_t}\nabla\overline{f'^2}\right) + C_g\mu_t\left(\nabla\overline{f}\right)^2 - C_d\rho\frac{\varepsilon}{k}\overline{f'^2} \tag{10}$$

$$\frac{\partial}{\partial t}\left(\rho\overline{H}\right) + \nabla\bullet\left(\rho\overrightarrow{v}\overline{H}\right) = \nabla\bullet\left(\frac{k_t}{c_p}\nabla\overline{H}\right) + S_h \tag{11}$$

All pre-processed values of the scalars temperature, species concentrations and density are related to the mixture fraction, mixture fraction variance and mean enthalpy calculated in the CFD code. The chemistry was reduced to a simple mixing problem in CFD without computationally demanding calculations. The settings for flamelet and PDF calculations are given in Table 5.

3.4. Radiation model

The RTE (radiative transport equations) were solved by the DO (discrete ordinates) model [65,66] with coefficients proposed by Smith et al. [41]. For the lab-scale furnace the DO model was already validated in Ref. [23]. The DO model solves the RTE for a finite number of discrete angles. A spatial discretization of 4 × 4 directions for each octant was used in CFD which results in an overall direction number of 128. Equation (12) shows the transfer equation where I is the radiation intensity, $\overrightarrow{r}$ is the position vector, $\overrightarrow{s'}$ is the scattering direction vector, σ_s stands for the scattering coefficient, Φ is the phase function and Ω' denotes the solid angle. Scattering coefficient and phase function were set to 0 1/m and isotropic respectively.

$$\nabla\bullet\left(I(\overrightarrow{r},\overrightarrow{s})\overrightarrow{s}\right) + (a+\sigma_s)I(\overrightarrow{r},\overrightarrow{s}) = an^2\frac{\sigma T^4}{\pi} + \frac{\sigma_s}{4\pi}\int_0^{4\pi} I(\overrightarrow{r},\overrightarrow{s'})\Phi(\overrightarrow{s}\bullet\overrightarrow{s'})d\Omega' \tag{12}$$

4. Results and discussion

4.1. Gas saving without thermal load

For future investigations on oxy-fuel combustion CFD calculations will be used to predict the combustion process and energetic efficiency without expensive tests on the furnaces. Thus, CFD was validated for different oxygen concentrations. This section

Table 5
Settings for flamelet and PDF calculation.

Flamelet calculation	
Maximum number of flamelets	20
Number of grid points in flamelet	32
Initial scalar dissipation (1/s)	0.01
Scalar dissipation step (1/s)	5
PDF calculation	
Number of mean mixture fraction points	40
Number of mixture fraction variance points	40
Minimum temperature (°C)	20
Number of mean enthalpy points	41

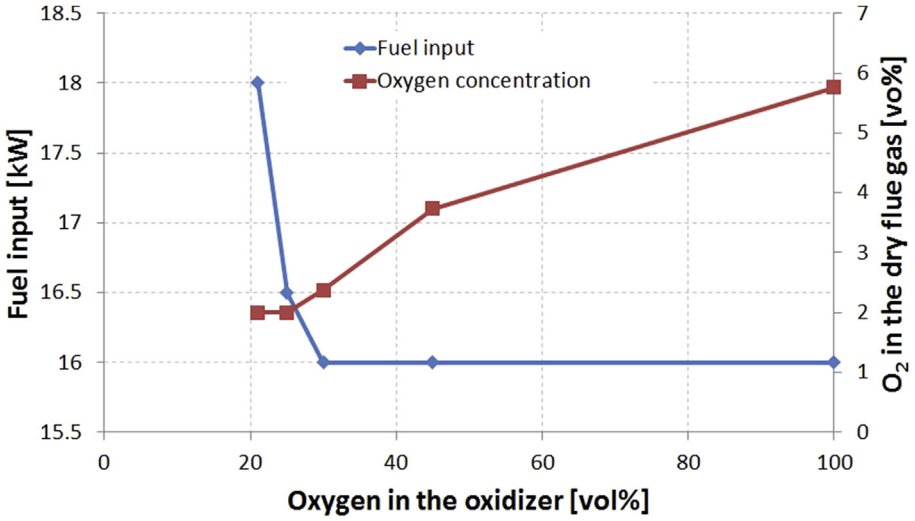

Fig. 4. Natural-gas input and oxygen content in the dry flue gas without thermal load.

comprises the results of the CFD simulation and experiments without thermal load. Test runs were carried out for 21, 25, 30, 45 and 100 vol% O_2 in the oxidizer to examine the gas savings potential of oxygen enriched combustion. Fuel input was adapted to achieve a measured temperature at T4 of 1090 °C. Fig. 4 shows the natural-gas needs and oxygen content in the dry flue gas. Although the furnace was operated under stoichiometric and fuel-rich conditions an oxygen concentration in the dry flue gas between 2 and 5.7 vol% was determined, which indicates air leakage. A fuel input of 18 kW was used for air-fired conditions. Increasing oxygen enrichment from 21 to 30 vol% leads to a reduction of fuel input to 16 kW. Additionally, decreasing fuel input causes a reduced mass-flow-rate of the flue gas as well as CO_2 emissions. It was expected that increasing oxygen levels would further improve fuel saving. But based on increasing air leakage, determined by higher O_2 concentrations in the flue gas, 16 kW fuel input was needed with O_2 enrichments of 45 and 100 vol% and no further improvement in gas savings were measured.

Fig. 5 highlights the comparison of the measured and predicted temperature in the furnace. Measurements revealed a highest temperature of 1156 °C at measurement position T2 for 100 vol% which was above burner 2 (see Fig. 5a). Other measured temperatures were in a range of 1081 and 1086 °C and consequently lower than the simulated temperatures. The reason for that is the cooler ambient air leaking into the furnace which leads to a lower gas temperature for T1, T3 and T4. This air leakage was not considered in the simulation. Although the measurement showed a deviation of approximately 40 K to the simulated values the numerical model can predict the oxy-fuel flame. Since T2 was measured in the vicinity of the flame, predicted and measured temperature are in close accordance because the flame, which is in the middle of the furnace, was hardly affected by the air leakage. A close accordance between the measurements and CFD was found for 21, 25, 30 and 45 vol% O_2 in the oxidizer where the air leakage was at a moderate level of 2–3.7 vol% (see Fig. 5b–e). The used CFD model slightly underestimates the temperature in the furnace for all measurement points (except 100 vol%) with a maximum deviation at T2 for 30 vol% of 27 K between CFD and measurement which is a good accordance and sufficient for predicting the temperature. A comparison between the measurements and CFD prediction revealed an average deviation of 16 K (except 100 vol%). Based on these results it was found, that the numerical model can predict the temperatures in the full range of oxygen enrichment with close agreement to experimental results, with a very low calculation time of three to four days. Also the used model is applicable without any changes or refinements on the reaction mechanism or model settings (see Refs. [18,51,53]). Similar EDC calculations with a 17 species mechanism were finished after 3 weeks on the same grid [23]. CFD prediction of the flame shapes and temperatures for burner 2 are displayed in Fig. 6. Due to the low nitrogen concentration in the oxidizer, temperatures higher than 1500 °C were calculated for 30, 45 and 100 vol%. Simulations with 25 and 21 vol% O_2 showed flame temperatures of approximately 1300–1450 °C.

The simulated heat losses through the outlet and outlet temperatures are displayed in Fig. 7. The air-fired experiment presents a heat loss through the outlet of 8 kW and a temperature of about 950 °C. So, compared to the fuel input of 18 kW, 45% of the power exits the furnace through the outlet. Change of radiative properties of the flue gas and flame temperature due to oxygen enrichment leads to a decreasing gas temperature at the outlet which also reduces heat loss. This loss was reduced to 1.84 kW for pure oxygen combustion which is beneficial for industrial processes like melting and annealing.

4.2. Furnace efficiency due to oxygen enrichment

Experiments and CFD simulations were carried out to investigate the furnace efficiency for two different temperature levels with thermal load inside. The heat transfer to the furnace load is a crucial part of optimization activities in several industrial processes like melting and annealing. Fuel input was adapted in the experiments to achieve 1000 and 1220 °C at measurement position T4 (see Fig. 8).

At a temperature level of 1000 °C the fuel input for 30, 45 and 100 vol% was quite similar with values between 41.7 and 43 kW. For air-fired conditions the fuel input was increased to 51 kW. With a thermal load, a gas saving of 8.2% was achieved for the same O_2 concentrations in the oxidizer. Further increase of the oxygen enrichment to 100 vol% showed a gas saving of 8.5 kW (or 16.7%), compared to air-firing. Experiments at 1220 °C were carried out for 30, 45 and 100 vol% O_2 only due to the restriction of the furnace equipment for the maximum fuel input. Fuel input for combustion with pure oxygen was 74.8 kW. For 30 vol% the fuel input was increased up to 98 kW to reach 1220 °C at measurement point T4. Such a large increase in the fuel input between 30 and 100 vol% was not observed at 1000 °C. This effect can be explained by the heat

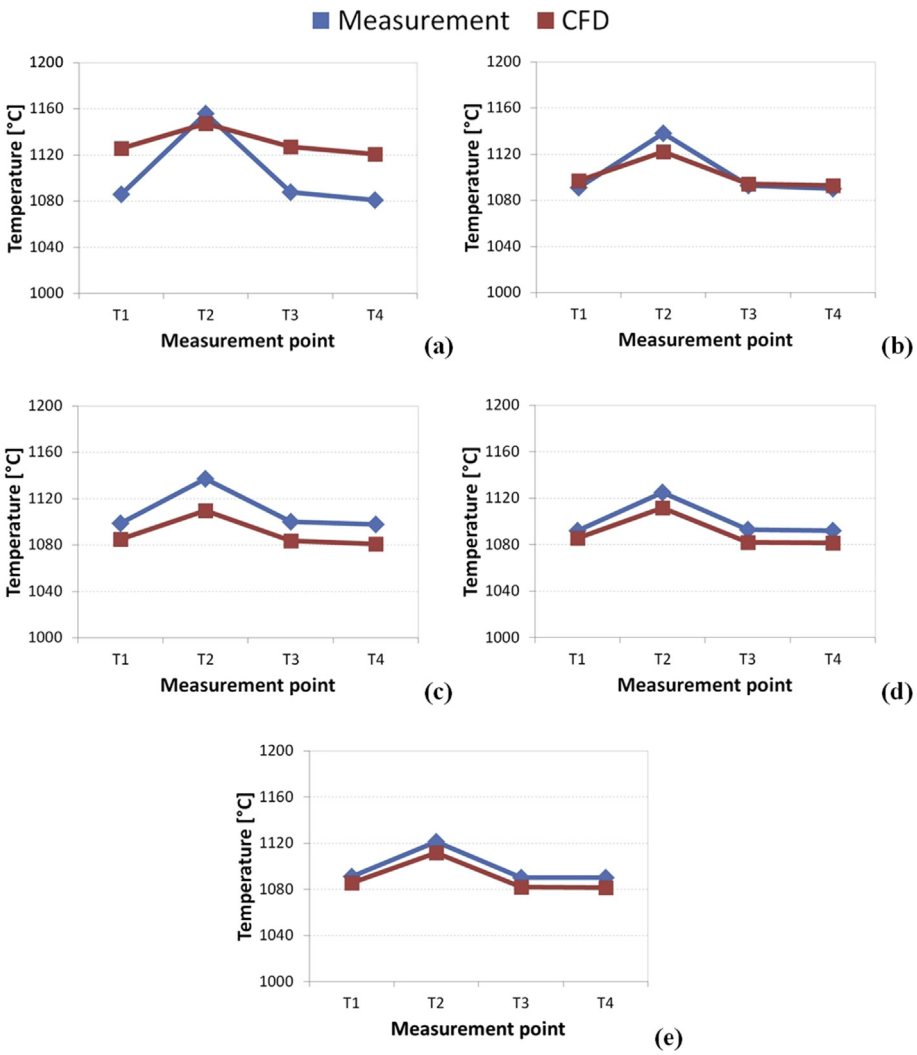

Fig. 5. Measured and calculated temperatures in the furnace: (a) 100 vol% O_2; (b) 45 vol% O_2; (c) 30 vol% O_2; (d) 25 vol% O_2; (e) 21 vol% O_2.

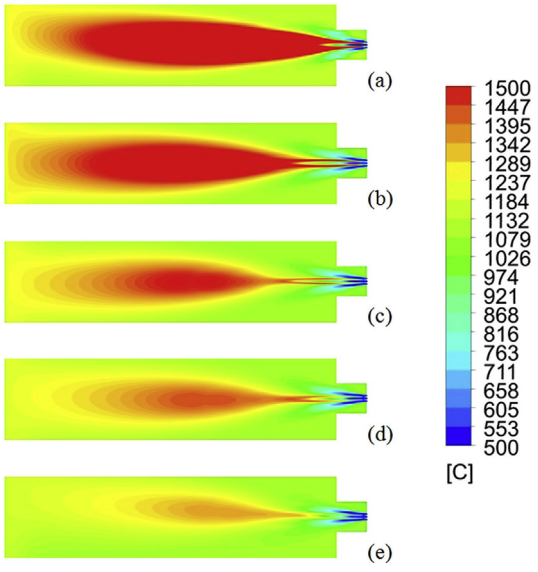

Fig. 6. Temperature plots of burner 2: (a) 100 vol%; (b) 45 vol%; (c) 30 vol%; (d) 25 vol %; (e) 21 vol%.

losses of the flue gas. The mass-flow-rate of the flue gas and calculated temperature at the outlet are displayed in Fig. 9. The outlet temperature of the flue gas was determined with 801 and 1025 °C for 100 vol% O_2. Both temperature levels showed a similar increase in the outlet temperature of approximately 100 °C between 30 and 100 vol%. However, the mass-flow-rate of the flue gas differs significantly. For example, with 30 vol% O_2 in the oxidizer mass-flow-rates of 43.7 and 102.4 kg/h were observed at the outlet, compared to 15.8 and 27.1 kg/h at 100 vol% O_2. The increasing nitrogen flow-rate is mostly responsible for the high mass-flow-rates at the outlet and heat losses through the flue gas.

Measured and predicted heat fluxes to the copper plate in the lab-scale furnace are displayed in Fig. 10 (left). Both experiments and CFD, showed that heat flux to the load increased by about 25 kW due to the higher temperature level. Heat fluxes were measured in the range of 20.4–22.8 kW (at 1000 °C) as well as 40.5–43 kW (at 1220 °C). A slight increase was determined in the heat fluxes from air-fired to oxy-fuel conditions which were caused by the higher radiative heat flux under an oxy-fuel environment. This heat transfer by radiation leads to a more homogeneous heat flux to the load and temperature distribution (see Prieler et al. [55]). The impact of the oxygen enrichment on the heat transfer to the load is essential for example the steel, glass, cement etc. industries to ensure the desired product quality. For industrial scale furnaces

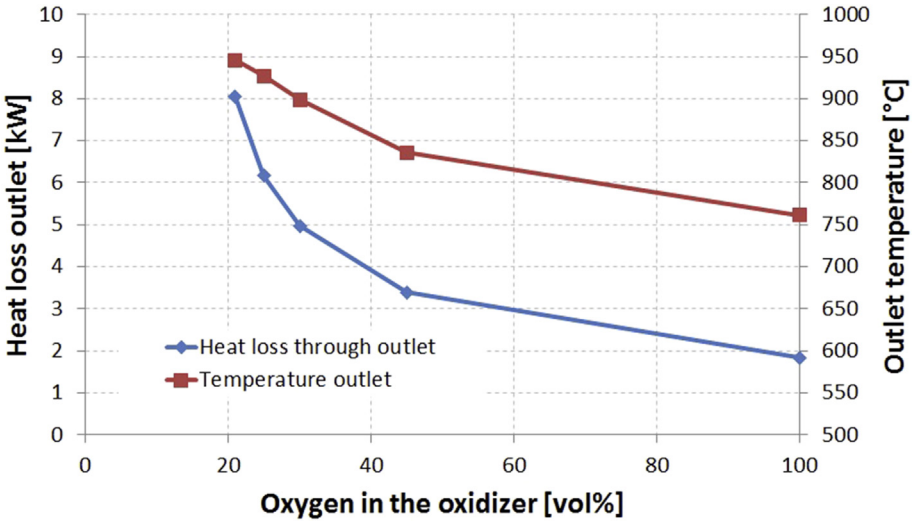

Fig. 7. Calculated outlet temperature depending on the oxygen concentration.

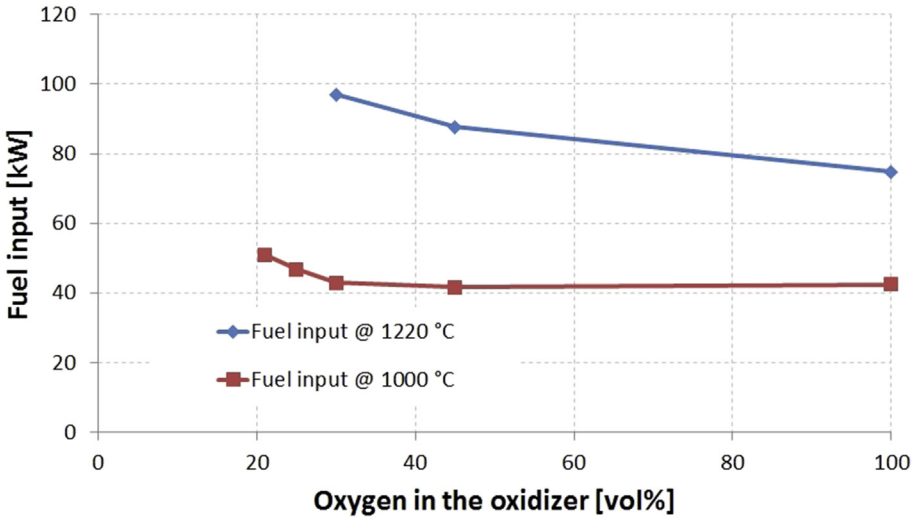

Fig. 8. Fuel input at 1000 and 1220 °C depending on the oxygen concentration.

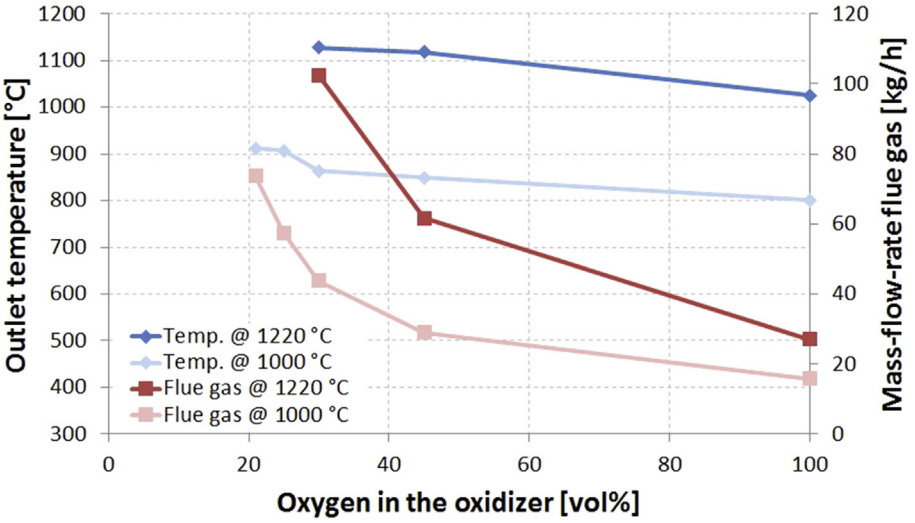

Fig. 9. Calculated outlet temperature and mass-flow-rate of the flue gas at 1000 and 1220 °C.

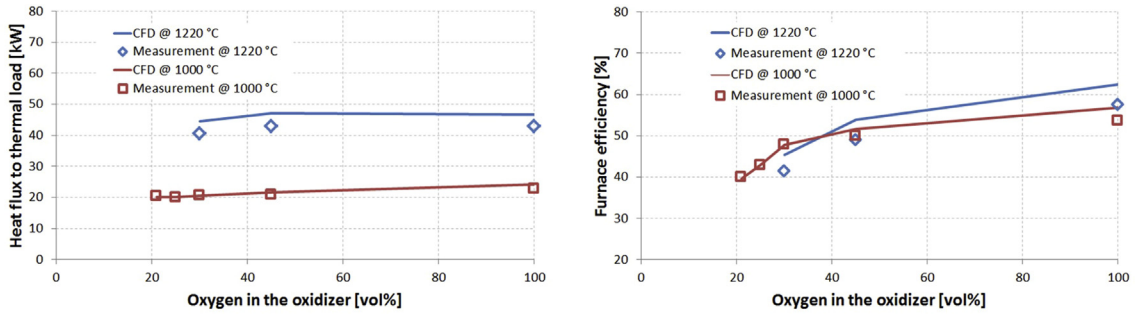

Fig. 10. Predicted and measured heat fluxes to furnace load (left) and furnace efficiencies (right) at 1000 °C and 1220 °C.

experiments to determine the heat fluxes on the load are very demanding. Therefore, CFD calculations offer an opportunity to predict local heat fluxes, temperatures and species concentrations without expensive experiments. Measurement and CFD were in good accordance at 1000 °C. The average deviation showed a value of 0.48 kW, which is a relative error of 1.7%. At 1220 °C higher deviations for all operating conditions were determined which were caused by higher air leakage during furnace operation. Experiments and simulation at 1220 °C showed an average deviation of 4 kW (9.5% relative error). Nevertheless, the predicted heat fluxes showed the same trend for the heat fluxes.

In Fig. 10 (right) the furnace efficiencies depending on the oxygen enrichment for 1000 and 1220 °C are displayed. The furnace efficiency is defined in Eq. (13), where $\dot{Q}_{load}$ is the total heat flux to the load and $\dot{Q}_{fuel}$ is the fuel input. Simulated and measured furnace efficiencies at 1000 °C are in close agreement and an increase in efficiency from 40 to 53.6% (measured) and 39.5–56.7% (CFD) was determined. Approximately 10% higher furnace efficiency was reached with 30 vol% O_2 instead of air-fired conditions. A mere 4–7% increase of furnace efficiency can be achieved from 30 to 100 vol% O_2. Maximum efficiency was observed at 1220 °C and 100 vol% O_2 with 57.5% (measured) and 62.5% (CFD). Despite the fact that higher values can be reached at 1220 °C, efficiency dropped faster with decreasing oxygen enrichment. Measurement revealed lower efficiency for 45 vol% O_2 with 49% compared to 1000 °C (49.9%). CFD simulation predicted that efficiency at 1220 °C drops below the efficiency at 1000 °C with an enrichment of 30 vol % O_2. Values of 45.4% (at 1220 °C) and 47.8% (at 1000 °C) were calculated.

$$\eta_{Furnace} = \frac{\dot{Q}_{load}}{\dot{Q}_{fuel}} \tag{13}$$

Based on the results, small oxygen enrichment levels in high temperature processes are more effective for higher temperatures. Burner adaptation for low enrichment levels of approximately 25 vol% can be done with little effort (oxygen supply and furnace equipment) and lead to improvements in the furnace efficiency. Calculated and predicted heat fluxes also showed a small increase of the heat flux to the furnace load. Furthermore, a comparison between CFD and measurements revealed that the CFD model that was used with the steady flamelet approach is able to predict the heat transfer in a lab-scale furnace with high accuracy. In contrast to the high calculation time for simulations with the commonly used EDC model, the steady flamelet approach was found to be a time saving method for CFD predictions of combustion processes. The computational time between a steady flamelet and an EDC simulation with reaction mechanisms containing 17 species was already tested by Prieler et al. [23,55].

4.3. Walking hearth furnace

It was pointed out in the last section as well as in Refs. [23] and [55], that the steady flamelet approach and the discrete ordinates model with the WSGG model can be applied for combustion modelling of air-fired and oxy-fuel conditions in lab-scale dimension. Although a detailed chemical kinetic with 17 species was used, the calculation time was reduced by solving only two additional transport equations for the turbulence/chemistry interaction. Calculation time for this industrial furnace was about 8 days on a standard 8 CPU-core workstation. In this section, an 18.2 MW walking hearth furnace was investigated using CFD to determine the heat fluxes to the steel billets inside the furnace. According to material data and production rate given in Section 2.2, an overall heat flux of 9.33 MW is required to achieve the desired billet temperature at the furnace outlet. Hence a furnace efficiency of 51.3% is reached for these operating conditions. The energetic efficiency of the lab-scale furnace was approximately 10% lower at 1000 °C due to air leakage and a slighter thickness of the furnace insulation. Fig. 11 shows the calculated temperatures in the furnace under air-fuel conditions. In the heating and soaking zone of the furnace a homogenous flue gas temperature between 1200 and 1350 °C was simulated. The pre-heating zone is approximately 200–300 °C colder than heating and soaking zone. The total and specific heat fluxes to the billets are displayed in Fig. 12. After entering the furnace, the heat flux to the billet was calculated with a value of about 144 kW. At 2200 mm the lowest heat flux of 90 kW occurs in the pre-heating zone. The maximum heat flux was simulated at the beginning of the heating zone with 262 kW. A simulation predicted a total heat flux to the billets of 9.15 MW compared to the 9.33 MW which are required. The deviation was 0.18 MW with a relative error of 1.9%.

The results highlighted the close accordance between CFD calculations and requirements. The furnace equipment and burner configuration that were used, can be applied for oxygen enrichment with simple modifications. Therefore, the CFD calculations presented in this paper will be the basis for further optimization activities regarding oxygen enrichment on this walking hearth furnace. Fuel savings will be predicted in CFD and compared to test runs on the walking hearth furnace.

5. Conclusion

In the present study the impact of air-fired and oxygen enriched combustion on fuel consumption and heat transfer in two furnaces was determined. Experiments on a lab-scale furnace were done with and without thermal load for 21, 25, 30, 45 and 100 vol% O_2 in the N_2/O_2 mixture which was used as oxidizer. Temperature and heat fluxes to the furnace load were measured to investigate the impact of oxygen enriched combustion on the fuel consumption

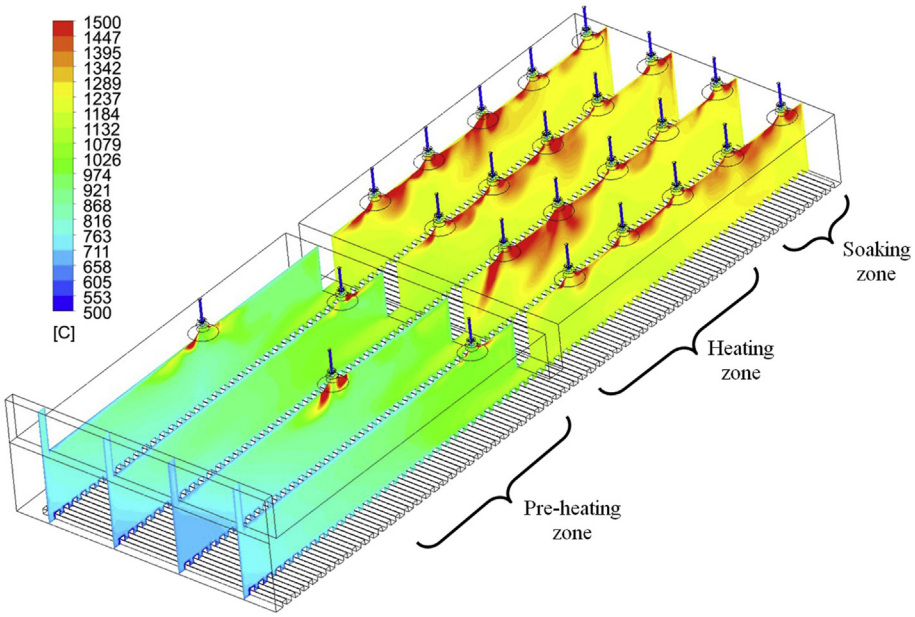

Fig. 11. Calculated temperature in the walking hearth furnace.

and furnace efficiency respectively. Apart from measurements, CFD simulations were carried out to validate the used models for combustion and radiation in an oxy-fuel environment. A reaction mechanism with 17 species and 25 reversible reactions was used in association with the steady flamelet approach. Although a detailed reaction mechanism with 17 species was applied, the calculation time for the lab-scale furnace was reduced to 3–4 days by the SFM. The WSGG model was used to calculate the radiative properties of the flue gas.

Without thermal load the test runs examined a gas saving potential 2 kW by using O_2 concentrations of 21 and 30 vol% in the oxidizer compared to air-fired conditions. Further improvements were not observed due to air leakage at 45 and 100 vol% O_2. Furthermore, a reduction of the heat loss through the outlet from 8 to 1.84 kW was determined. Temperature measurements inside the furnace revealed close agreement with the CFD prediction with an average deviation of 16 K for all cases. It was found that the, CFD model can be applied for all oxygen enrichments in this furnace without changes on the model settings and reaction mechanism.

With thermal load two temperature levels of 1000 and 1220 °C were investigated through experiments and simulation. Results, which were similar to tests without load, showed a gas saving of 8.2% with 25 vol% O_2. A greater gas saving potential due to oxy-fuel combustion was identified at a higher temperature level in the furnace. Crucial for its application in annealing and melting furnaces is the heat flux to the furnace load. Measured and calculated heat fluxes to the thermal load were compared and were in close agreement with an average relative error of 0.48 kW (at 1000 °C) and 4 kW (at 1220 °C). The higher difference at 1220 °C was attributed to higher air leaking during the experiments. Heat fluxes to the load were determined with 20.4–22.8 kW at 1000 °C whereas the heat flux was doubled by increasing the temperature

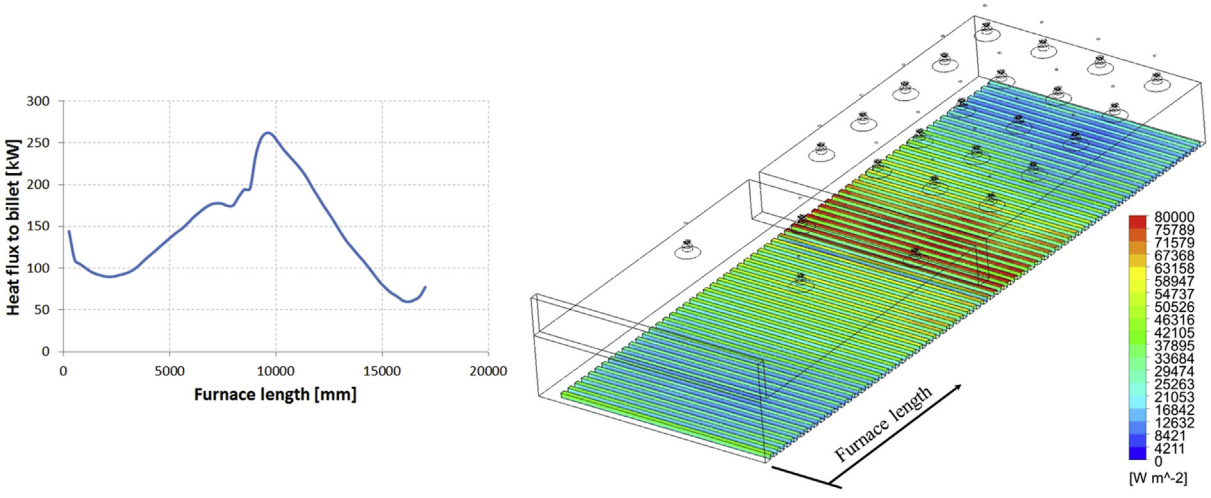

Fig. 12. Heat fluxes to the billets: heat flux (left); Contour plot of the specific heat flux at the billet surface (right).

to 1220 °C. It was also found, that furnace efficiency was increased by 13.6% with combustion of pure oxygen compared to air-fired conditions.

Based on the results for the lab-scale furnace, the CFD approach that was used is capable of predicting temperature and heat fluxes in high temperature furnaces. Therefore an 18.2 MW walking hearth furnace for reheating steel billets was numerically investigated. Currently the furnace operates under air-fired conditions. The CFD simulation predicted the total heat flux to the steel billets as 9.15 MW in contrast to 9.33 MW which are required according to material data and production rate. So, there was a relative error of 1.9% which is a good approximation and sufficient to simulate industrial furnaces. CFD also represents the only method to determine local temperatures and species concentrations in the furnace. This is the basis for further optimization activities at the walking hearth furnace. A numerical study with oxygen enriched combustion and minor modifications on the furnace will be done in order to carry out test runs on the furnace.

Acknowledgement

This work was financially supported by FFG, “Competence-Headquarter: Nachhaltige Prozessoptimierung durch Verbrennung mit Sauerstoff” (project 839616, eCall 3392435) with co-financing by EFRE (“Europäischer Fonds für regionale Entwicklung”).

Appendix

Table 6
List of reactions and species for the reaction mechanism skeletal25.

Number	Reaction
1	$H + O_2 \leftrightarrow O + OH$
2	$O + H_2 \leftrightarrow O + OH$
3	$H_2 + OH \leftrightarrow H_2O + H$
4	$OH + OH \leftrightarrow H_2O + O$
5	$H + O_2 + M \rightarrow HO_2 + M$
6	$H + HO_2 \rightarrow OH + OH$
7	$H + HO_2 \rightarrow H_2 + O_2$
8	$OH + HO_2 \rightarrow H_2O + O_2$
9	$CO + OH \leftrightarrow CO_2 + H$
10	$CH_4 \leftrightarrow CH_3 + H$
11	$CH_4 + H \leftrightarrow CH_3 + H_2$
12	$CH_4 + OH \leftrightarrow CH_3 + H_2O$
13	$CH_3 + O \rightarrow CH_2O + H$
14	$CH_2O + H \rightarrow HCO + H_2$
15	$CH_2O + OH \rightarrow HCO + H_2O$
16	$HCO + H \rightarrow CO + H_2$
17	$HCO + M \rightarrow CO + H + M$
18	$CH_3 + O_2 \rightarrow CH_3O + O$
19	$CH_3O + H \rightarrow CH_2O + H_2$
20	$CH_3O + M \rightarrow CH_2O + H + M$
21	$HO_2 + HO_2 \rightarrow H_2O_2 + O_2$
22	$H_2O_2 + M \leftrightarrow OH + OH + M$
23	$H_2O_2 + OH \leftrightarrow H_2O + HO_2$
24	$OH + H + M \rightarrow H_2O + M$
25	$H + H + M \rightarrow H_2 + M$

List of Species: H_2, O_2, O, H, OH, H_2O, HO_2, CO, CO_2, CH_4, CH_3, CH_2O, HCO, CH_3O, $H2O_2$, N_2, N.

References

[1] Intergovernmental Panel on Climate Change (IPPC). IPPC special report on carbon dioxide capture and storage. Cambridge, UK and New York, NY, USA: Cambridge University Press; 2005.
[2] Manickam B, Dinkelacker F, Lobe T, Tertychnyy M. Enriched oxygen combustion simulation for rotary kiln application. In: 4th European Combustion Meeting, Vienna, Austria; 2009.
[3] Falcitelli M, Pasini S, Tognotti L. Modelling practical combustion systems and predicting NOx emissions with an integrated CFD based approach. Comput Chem Eng 2002;26:1171–83.
[4] Chen L, Yong SZ, Ghoniem AF. Oxy-fuel combustion of pulverized coal: characterization, fundamentals, stabilization and CFD modeling. Prog Energy Comb Sci 2012;38:156–214.
[5] Scheffknecht G, Al-Makhadmeh L, Schnell U, Maier J. Oxy-fuel coal combustion—A review of the current state-of-the-art. Int J Greenh Gas Control 2011;5:16–35.
[6] Wall T, Liu Y, Spero C, Elliott L, Khare S, Rathnam R, et al. An overview on oxyfuel coal combustion—state of the art research and technology development. Chem Eng Res Des 2009;87:1003–16.
[7] Oliveira FAD, Carvalho JA, Sobrinho PM, de Castro A. Analysis of oxy-fuel combustion as an alternative to combustion with air in metal reheating furnaces. Energy 2014;78:290–7.
[8] Bělohradský P, Skryja P, Hudak I. Experimental study on the influence of oxygen content in the combustion air on the combustion characteristics. Energy 2014;75:116–26.
[9] Baukal CE. Oxygen-enhanced combustion. 2nd ed. Boca Raton: CRC Press; 2013.
[10] Ponsich A, Azzaro-Pantel C, Domenech S, Pibouleau L, Pigeonneau F. A systemic approach for glass manufacturing process modeling. Chem Eng Proc Process Intensif 2009;48:1310–20.
[11] Habibi A, Merci B, Heynderickx GJ. Multiscale modeling of turbulent combustion and NO_x emission in steam crackers. AIChE J 2007;53:2384–98.
[12] Guihua H, Honggang W, Feng Q. Numerical simulation on flow, combustion and heat transfer of ethylene cracking furnaces. Chem Eng Sci 2011;66:1600–11.
[13] Furu J, Buchholz A, Bergstrøm HT, Marthinsen K. Numerical modeling of oxy-fuel and air-fuel burners for aluminium melting. In: Light metals 2012. Hoboken, NJ, USA: John Wiley & Sons, Inc; 2012.
[14] Smith GP, Golden DM, Frenklach M, Moriarty NW, Eiteneer B, Goldenberg, MC, Bowman T, Hanson RK, Song S, Gardiner Jr WC, Lissianski VV, Qin Z. http://www.me.berkeley.edu/gri_mech/.
[15] Westbrook CK, Dryer FL. Simplified reaction mechanisms for the oxidation of hydrocarbon fuels in flames. Combust Sci Technol 1981;27:31–43.
[16] Jones WP, Lindstedt RP. Global reaction schemes for hydrocarbon combustion. Combust Flame 1988;73:233–49.
[17] Frassoldati A, Cuoci A, Faravelli T, Ranzi EM, Candusso C, Tolazzi D. Simplified kinetic schemes for oxy-fuel combustion. In: Proceedings of S4FE2009-International Conference on Sustainable Fossil Fuels for Future Energy, Rome, Italy; 2009.
[18] Yin C, Rosendahl LA, Kær SK. Chemistry and radiation in oxy-fuel combustion: a computational fluid dynamics modeling study. Fuel 2011;90:2519–29.
[19] Glarborg P, Bentzen LLB. Chemical effects of a high CO_2 concentration in oxy-fuel combustion of methane. Energy Fuels 2008;22:291–6.
[20] Andersen J, Rasmussen CL, Giselsson T, Glarborg P. Global combustion mechanisms for use in CFD modeling under oxy-fuel conditions. Energy Fuels 2009;23:1379–89.
[21] Tihay V, Santoni P-A, Simeoni A, Garo J-P, Vantelon J-P. Skeletal and global mechanisms for the combustion of gases released by crushed forest fuels. Combust Flame 2009;156:1565–75.
[22] Peters N, Kee RJ. The computation of stretched laminar methane-air diffusion flames using a reduced four-step mechanism. Combust Flame 1987;68:17–29.
[23] Prieler R, Demuth M, Spoljaric D, Hochenauer C. Evaluation of a steady flamelet approach for use in oxy-fuel combustion. Fuel 2014;118:55–68.
[24] Peeters TWJ. Numerical modeling oft turbulence natural-gas diffusion flames (PhD Thesis). Delft, The Netherlands: Delft Technical University; 1995.
[25] Kutne P, Kapadia BK, Meier W, Aigner M. Experimental analysis of the combustion behaviour of oxyfuel flames in a gas turbine model combustor. Proc Combust Inst 2011;33:3383–90.
[26] Hottel HC, Sarofim AF. Radiative transfer. New York: McGraw-Hill; 1967.
[27] Porter R, Liu F, Pourkashanian M, Williams A, Smith D. Evaluation of solution methods for radiative heat transfer in gaseous oxy-fuel combustion environments. J Quant Spect Rad Trans 2010;111:2084–94.
[28] Modest MF. Radiative heat transfer. 3rd ed. Boston: Academic Press; 2013.
[29] Modest MF. Narrow-band and full-spectrum k-distributions for radiative heat transfer – correlated-k vs. scaling approximation. J Quant Spect Rad Trans 2003;76:69–83.
[30] Modest MF, Zhang H. The full-spectrum correlated-k distribution for thermal radiation from molecular gas-particulate mixtures. ASME J Heat Trans 2002;124:30–8.
[31] Goody RM. A statistical model for water-vapour absorption. Q J R Meteorol Soc 1952;78:165–9.
[32] Becher V, Clausen S, Fateev A, Spliethoff H. Validation of spectral gas radiation models under oxyfuel conditions. Part A: gas cell experiments. Int J Greenh Gas Control 2011;5:76–99.
[33] Becher V, Goanta A, Spliethoff H. Validation of spectral gas radiation models under oxyfuel conditions – part C: validation of simplified models. Int J Greenh Gas Control 2012;11:34–51.
[34] Rothman LS, Gordon IE, Barber RJ, Dothe H, Gamache RR, Goldman A, et al. HITEMP, the high-temperature molecular spectroscopic database. J Quant Spect Rad Trans 2010;111:2139–50.

[35] Rothman LS, Wattson RB, Gamache R, Schroeder JW, McCann A. HITRAN HAWKS and HITEMP: high-temperature molecular database. In: Proc SPIE 2471, atmospheric propagation and remote sensing IV; 1995.
[36] Rothman LS, Gordon IE, Barbe A, Benner DC, Bernath PF, Birk M, et al. The HITRAN 2008 molecular spectroscopic database. J Quant Spect Rad Trans 2009;110:533–72.
[37] Rothman LS, Jacquemart D, Barbe A, Benner DC, Birk M, Brown LR, et al. The HITRAN 2004 molecular spectroscopic database. J Quant Spect Rad Trans 2005;96:139–204.
[38] Grosshandler W. RADCAL: a narrow-band model for radiation calculations in a combustion environment. Gaitherburg: National Institute of Standards and Technology; 1993.
[39] Soufani A, Taine J. High temperature gas radiative property parameters of statistical narrow-band model for H_2O, CO_2 and CO, and correlated-k model for H_2O and CO_2. Int J Heat Mass Trans 1997;40:987–91.
[40] Edwards DK. Molecular gas band radiation. Adv Heat Transf 1976;12:115–93.
[41] Smith TF, Shen ZF, Friedman JN. Evaluation of coefficients for the weighted sum of gray gases model. J Heat Trans 1982;104:602–8.
[42] Yin C, Johansen LCR, Rosendahl LA, Kær SK. New weighted sum of gray gases model applicable to computational fluid dynamics (CFD) modeling of oxy–fuel combustion: derivation, validation, and implementation. Energy Fuels 2010;24:6275–82.
[43] Edwards DK, Balakrishnan A. Thermal radiation by combustion gases. Int J Heat Mass Trans 1973;16:25–40.
[44] Johansson R, Andersson K, Leckner B, Thunman H. Models for gaseous radiative heat transfer applied to oxy-fuel conditions in boilers. Int J Heat Mass Transf 2010;53:220–30.
[45] Johansson R, Leckner B, Andersson K, Johnsson F. Account for variations in the H_2O to CO_2 molar ratio when modelling gaseous radiative heat transfer with the weighted-sum-of-grey-gases-model. Combust Flame 2011;158:893–901.
[46] Bordbar MH, Wecel G, Hyppänen T. A line by line based weighted sum of gray gases model for inhomogeneous CO_2-H_2O mixture in oxy-fired combustion. Combust Flame 2014;161:2435–45.
[47] Rehfeldt S, Kuhr C, Ehmann M, Bergins C. Modeling of radiative properties of an oxyfuel atmosphere with a weighted sum of gray gases for variable carbon dioxide and water vapor concentrations. Energy Procedia 2011;4:980–7.
[48] Kangwanpongpan T, Franca FHR, Correa da Silva R, Schneider PS, Krautz HJ. New correlations for the weighted-sum-of-gray-gases model in oxy-fuel conditions based on HITEMP 2010 database. Int J Heat Mass Transf 2012;55:7419–33.
[49] Krishnamoorthy GA. new weighted-sum-of-gray-gases model for CO_2-H_2O gas mixtures. Int Commun Heat Mass Transf 2010;37:1182–6.
[50] Kim JP, Schnell U, Scheffknecht G. Comparison of different global reaction mechanisms for MILD combustion of natural gas. Combust Sci Technol 2008;180:565–92.
[51] Al-Abbas AH, Naser J. Numerical study of one air-fired and two oxy-fuel combustion cases of propane in a 100 kW furnace. Energy Fuels 2012;26:952–67.
[52] Al-Abbas AH, Naser J. Effect of chemical reaction mechanisms and NOx modeling on air-fired and oxy-fuel combustion of lignite in a 100-kW furnace. Energy Fuels 2012;26:3329–48.
[53] Galletti C, Coraggio G, Tognotti L. Numerical investigation of oxy-natural-gas combustion in a semi-industrial furnace: validation of CFD sub-models. Fuel 2013;109:445–60.
[54] Coppalle A, Vervisch P. The total emissivities of high-temperature flames. Combust Flame 1983;49:101–8.
[55] Prieler R, Demuth M, Spoljaric D, Hochenauer C. Numerical investigation of the steady flamelet approach under different combustion environments. Fuel 2015;140:731–43.
[56] Shih T-H, Liou WW, Shabbir A, Yang Z, Zhu J. A new k-ε eddy viscosity model for high reynolds number turbulent flows – model development and validation. Comp Fluids 1995;24(3):227–38.
[57] Launder BE, Reece GJ, Rodi W. Progress in the development of a Reynolds-stress turbulence closure. J Fluid Mech 1975;68(3):537–66.
[58] Yin C. Advanced modeling of oxy-fuel combustion of natural-gas. ForskEL report 2009-1-0256. 2011. Online:, http://energinet.dk/SiteCollectionDocuments/Danske%20dokumenter/Forskning%20-%20PSO-projekter/10256%20Advanced%20modeling%20of%20oxy-fuel%20combustion%20of%20natural%20gas.pdf.
[59] Richardson LF. The approximate arithmetical solution by finite differences of physical problems involving differential equations, with an application to the stresses in a masonry dam. Trans R Soc Lond Ser A 1910;210:307–57.
[60] Magnussen BF, Hjertager BH. On mathematical modeling of turbulent combustion with special emphasis on soot formation and combustion. In: 16th Symposium (Int) on Combustion. The Combust Inst; 1976.
[61] Magnussen BF. On the structure of turbulence and a generalized eddy dissipation concept for chemical reaction in turbulent flow. In: 19th AIAA Meeting. St. Louis, USA; 1981.
[62] Peters N. Laminar diffusion flamelet models in non-premixed turbulent combustion. Prog Energy Combust Sci 1984;10:319–39.
[63] Peters N. Laminar flamelet concepts in turbulent combustion. In: 21st Symposium (Int) on Combustion. The Combust Inst; 1986. p. 1231–50.
[64] Jones WP, Whitelaw JH. Calculation methods for reacting turbulent flows: a review. Combust Flame 1982;48:1–26.
[65] Chui EH, Raithby GD. Computation of radiant heat transfer on a non-orthogonal mesh using the finite-volume method. Numer Heat Transf Part B Fundam 1993;23:269–88.
[66] Raithby GD, Chui EH. A finite-volume method for predicting a radiant heat transfer in enclosures with participating media. J Heat Transf 1990;112:415–23.